Supporting Information

Tuning Hybridization and Charge Polarization in Metal Nanoparticles Dispersed over Schiff Base Functionalized SBA-15 Enhances CO_2 Capture and Conversion to Formic Acid

Arjun Cherevotan[1,2], Bitan Ray[1,2#], Anish Yadav[1,2#], Debabrata Bagchi[1,2], Ashutosh Kumar Singh,[2,3] Sathyapal R. Churipard[1,2], Mohd Riyaz[1,2], Vinay Naral[1,2], Komalpreet Kaur,[4] Ujjal K. Gautam,[4] Chathakudath P. Vinod,[5] and Sebastian C. Peter[1,2]*

[1]New Chemistry Unit, Jawaharlal Nehru Centre for Advanced Scientific Research, Jakkur, Bangalore-560064
[2]School of Advanced Materials, Jawaharlal Nehru Centre for Advanced Scientific Research, Jakkur, Bangalore-560064
[3]Chemistry and Physics of Materials Unit, Jawaharlal Nehru Centre for Advanced Scientific Research, Jakkur, Bangalore-560064
[4]Department of Chemical Sciences, Indian Institute of Science Education and Research (IISER)-Mohali, Sector 81, Mohali, SAS Nagar, Punjab, 140306
[5]Catalysis and Inorganic Chemistry Division, CSIR-National Chemical Laboratory, Pune 410008
**Email: sebastiancp@jncasr.ac.in, sebastiancp@gmail.com,* Phone: 080-22082998, Fax: 080-22082627
# Authors contributed equally

Experimental Section

Materials

Pluronic P123 (Mn~5800, Sigma Aldrich), cetyltrimethylammonium bromide (CTAB), tetraethylorthosilicate (TEOS) (>99% GC, Sigma Aldrich), H_2SO_4 (98% analytical grade, Merck Chemicals), ethanol, dry toluene, (3-aminopropyl) triethoxysilane [APTES] were used as purchased without any further purification except toluene. Molecular sieves were heated at 200 °C and commercially procured toluene was poured to it slowly. Using this process toluene was dried and water-free, and it was stored and kept for further synthetic application.

Synthesis

SBA-15: The support material Santa Barbara Amorphous (SBA-15) was synthesized by modifying an already reported method.[1, 2] Four grams of Pluronic P123 was dissolved in 105 mL of deionized (DI) water and 10.8 ml of 98% H_2SO_4 to act as a soft template. Then 9.063 mL of TEOS was added to the solution with a high rate of stirring for 3.5 hours at 313 K, followed by hydrothermal treatment at 373 K for 30 hours. The obtained white powder was filtered, washed with DI water, dried at 373 K overnight and was calcined for 6 hours at 823 K.

APTES-Aldehyde/SBA15 (Direct Method): 1.5 g of as synthesized SBA-15 was suspended in dry toluene; amine loading was conducted via the addition of 2.4 ml APTES and 9.82 ml of the respective aldehyde in complete inert condition using nitrogen to make sure there is no oxidation of APTES prior to amine grafting. The mixture was stirred at 40 °C overnight in the nitrogen atmosphere. The resulting compound was dried overnight at 60 °C.

APTES-Aldehyde/SBA15 (Indirect Method): The as synthesized SBA-15 (1.5 g) was suspended in dry toluene; amine loading was conducted via the addition of 2.4 ml APTES in complete inert condition using the nitrogen atmosphere. The mixture was stirred at 40 °C overnight in the nitrogen atmosphere. The resulting compound (APTES/SBA-15) was dried overnight at 60 °C. APTES (0.5 g) grafted SBA-15 (APTES/SBA-15) was dispersed in 20 ml

deionized water and 6.61 ml of the respective aldehyde was slowly added under constant stirring. Hydrothermal treatment of the mixture was done using a 50 ml autoclave at 150 ℃ for 12 hours. The resulting compound was filtered and washed using deionized water and further dried overnight at 60 ℃. Glutaraldehyde and Butyraldehyde were used in this reaction for the condensation of amines.

Metal nanoparticle incorporation to functionalised support: The metal nanoparticles were incorporated by following previous report.[3] 0.2 g of respective APTES-Aldehyde/SBA15 (Direct) was suspended in 50 ml deionized water and stirred for 10 mins. The nitrate salts of Pd and Ni/Ag/Co were weighed to get respective loading concentration and stirred for 30 mins. The metal nitrates were reduced using $NaBH_4$ addition ($NaBH_4$/metal mole ratio equivalent to 10:1) and stirred for another 30 mins. The resulting precipitate was filtered and washed using DI water. A similar method was used for the metal impregnation on Aldehyde/APTES/SBA-15 (Indirect method) and other supports. For better reactivity comparison different ratio of Pd to Ni/Ag combinations were also used. The schematic representation of the procedure is given in **Figure 1**. Monometallic Pd, Ni, Ag and Co were also synthesized by same metal incorporation synthetic steps taking respective concentration of their nitrate salt solution.

Material Characterisation

Inductively Coupled Plasma – Optical Emission Microscope (ICP-OES): ICP-OES was performed using a Perkin Elmer Optima 7000 DV instrument. The samples were first digested in concentrated aqua regia prepared in the lab by mixing four volumes of HNO_3 with one volume of HCl. Then samples were treated with 20-30 microliter of concentrated HF to remove silica of SBA-15 and finally diluted with distilled water. In a typical experiment, 5 mg of the sample was dissolved in 3-5 ml aqua regia and heated at 333 K for digestion. The digested sample was then treated with 40-50 microliter of concentrated HF and diluted to 10 ml volume with deionized water, from this 1 ml was again taken and diluted to 10 ml. The solid particles were separated by thorough centrifugation before measurements.

Fourier Transformed Infrared (FTIR): FTIR spectra were recorded with Perkin Elmer L125000P in the mid-IR region ($\bar{\upsilon}$ = 4000–400 cm^{-1}) using the powdered samples. The functionalised silica as well as the aldehyde condensed samples were analysed, and functional groups are confirmed using the standard wavenumber values available in literature.

X-ray Photoelectron Spectroscopy (XPS): XPS measurements were carried out using Thermo K-alpha+ spectrometer using micro focused and monochromated Al Kα radiation with energy 1486.6 eV. The pass energy for spectral acquisition was kept at 50 eV for individual core-levels. The electron flood gun was utilized for providing charge compensation during data acquisition. Further, the individual core-level spectra were checked for charging using C1s at 284.6 eV as standard and corrected if needed. The peak fitting of the individual core-levels was done using CasaXPS software with a Shirley type background.

XRD: The phase formation on SBA-15 was confirmed by X-ray diffraction (XRD) collected on PANalytical X-ray diffractometer with Cu Kα radiation at 45 kV and 40 mA. The XRD were acquired at a scan rate of 1.33 degree/min in an angle range of 10 to 90 degrees of 2q. The features of the PXRD patterns were compared with simulated pattern from Pearson Database. The catalysts powder XRD were compared with simulated phases of cubic Ag (S.G: $Fm\bar{3}m$), Pd (S.G: $Fm\bar{3}$m) and Ni (S.G: $Fm\bar{3}$m).

N_2 adsorption isotherms: The adsorption isotherms were studied by using N_2 at 77 K on BELSORP max II analyzer. Prior to the measurements, the powders were treated for degassing at 423 K for 6 hours. The specific surface area was confirmed by Brunaur-Emmett-Teller (BET) method and pore size distribution by classical BJH (Barrett, Joyner and Halenda)

method. The N_2 adsorption-desorption experiment exhibits type IV isotherm (Brunauer definition) with hysteresis loop, typical of hexagonal and cylindrical mesoporous materials. There is a fast increase in adsorption volume between 0.6-0.8 p/p0 which is indicative of capillary condensation attributed to the pre-formation of N_2 on the pore walls due to multilayer adsorption. The metal impregnated samples exhibited a left shift of the sharp rise in the adsorption isotherms and drastically diminished surface areas. This lowering of surface area concludes that impregnated clusters decrease the N_2 probing surface inside the mesopores.

Transmission Electron Microscope (TEM): TEM images and selected area electron diffraction patterns were collected using a JEOL JEM-2010 TEM instrument and color mapping was done in TECHNAI. The samples for these measurements were prepared by sonicating the nanocrystalline powders in ethanol and drop-casting a small volume onto a carbon-coated copper grid.

X-ray absorption (XAS): Measurements of Pd-*K*, Ni-*K* and Ag-*K* edges at ambient pressure were performed in fluorescence as well as transmission mode using gas ionization chambers to monitor the incident and transmitted X-ray intensities. at PETRA III, P64 beamline of DESY, Germany. Monochromatic X-rays were obtained using a Si (111) double crystal monochromator, which was calibrated by defining the inflection point (first derivative maxima) of Cu foil as 8980.5 eV. The beam was focused by employing a Kirkpatrick-Baez (K-B) mirror optic. Rhodium-coated X-ray mirror was used to suppress higher-order harmonics. A CCD detector was used to record the transmitted signals. Pellets for the ex-situ measurements were made by homogeneously mixing the sample with an inert cellulose matrix to obtain an X-ray absorption edge jump close to one. The XAS data processing were done using the ATHENA[4] software. The multiple data were collected and averaged out before proceeding to the background correction. The averaged data were smoothed out using the standard kernel size of 11. The weak spline was used for background correction in the pre-edge region. All the data were normalized for the Standard data analysis procedure was used to extract the extended X-ray absorption fine structure (EXAFS) signal from the measured absorption spectra.

CO_2 Capture test

Dynamic experiment is a preliminary experiment for initial screening and obtain the overall uptake capacity of any adsorbent material. Similar information can also be determined from thermogravimetric analysis or even CO_2 adsorption isotherm in physisorption analyser as well. However, in both the cases, it is very difficult to foresee the sorption ability or uptake capacity in real time scenario, as both the cases the experiment is performed in very confined and near ideal situation. Overall adsorption kinetics of the material can only be observed from the dynamic experiment. Breakthrough region is also considered as a measure of the material to be translated into commercial scale.

Dynamic Uptake Experiment: To perform the dynamic uptake experiment, sample were taken in a quartz tube, and simulated gas cylinder (5000 ppm CO_2 balanced with air) was connected to it and gas is allowed to pass through the adsorbent bed at 800 ml/min flow rate. The outlet of the quartz tube is connected to an IR-based gas analyser LI COR (LI-850) to sense the CO_2 (**Figure S2**). The experiment is performed till the saturation of material.

In order to calculate the uptake, the relative CO_2 concentration (C_t/C_0) is plotted against the time, where C_t represent the outlet concentration of CO_2 at time t, and C_0 is the CO_2 concentration of simulated gas cylinder. Breakthrough point is defined as the duration till material is sustained to adsorb CO_2 at its full efficiency. After that adsorption capacity is decreased, and slowly the material moves towards the saturation. (**Figure S3**)

The uptake value till breakthrough point can be calculated straight forward using the conventional equation, (**Eqn. 1**)

$$q_b = \frac{F \times C_0 \times t_b}{W} \qquad \ldots\ldots\ldots (1)$$

q_b is the uptake capacity till breakthrough point. F is the flow rate (ml/s), C_0 is the concentration of CO_2 inside simulated gas cylinder, t_b is breakthrough time (s), W is the mass of adsorbent (g). Thus, the q_b can be obtained in terms of ml of CO_2 per g of sorbent, which can also be converted to mg of CO_2 per g of sorbent. (CO_2; 1 mole ≡ 44.01 g ≡ 22400 ml)

Even after the breakthrough point, the CO_2 adsorption occur with a lesser efficiency when it is compared to the breakthrough region. In order to calculate the uptake for that particular region, Avrami kinetics model has been used, which considers multiple adsorption pathways. (**Eqn. 2**) Considering this model, the uptake is considered from breakthrough point to exhaustion point (C_t/C_0 is 0.9). [5] The value has been taken based on criterion that the adsorption kinetics is very slow after 0.9 value and extrapolated that the uptake is too negligible to consider. Hence in the conventional equation, time can be replaced with stoichiometric time to calculate CO_2 uptake. (**Eqn. 3**) As the plot is considered for C_t/C_0 vs time, C_t/C_0 is an unitless entity, hence the product is nothing but the time.

$$q_a = \frac{F \times C_0 \times t_q}{W} \qquad \ldots\ldots\ldots (2)$$

$$t_q = \int_{t_b}^{t_{ex}} \left(1 - \frac{C_t}{C_0}\right).dt \qquad \ldots\ldots\ldots (3)$$

t_q is the stoichiometric time, t_{ex} is exhaustion time, t_b is the breakthrough time. C_t is concentration of CO_2 at t time. The overall uptake for the adsorbent material can be considered as the sum of q_b and q_a. (**Eqn. 1** & **Eqn. 2**).

Static Uptake Experiment: The static uptake experiment was performed via BELSORP max II analyzer using CO_2 gas as the adsorbate. For the desired experiment two different temperatures were taken into consideration; one being 40 ℃ to mimic the experimental condition as implemented for the batch process CO_2 hydrogenation, and another is 0 ℃ or 273 K.

During the experiment small amount of sample (200 – 500 mg) was weighed and transferred into sample tube and vacuumized thoroughly at 50 ℃ for 12 hours to ensure maximum degassing without degrading the amine part present in the samples, prior to the experiment. The temperatures 40 ℃ and 0 ℃ were maintained using water and methanol respectively, taken into solvent bath.

CO_2 Conversion test

CO_2 reduction efficiency of the catalyst in liquid phase was screened by a batch Parr reactor. The parr Vessel's inside lining was prone to corrosion due to usage of basic and acidic solvents, thereby, 10 ml capacity quartz vials, enclosed with rubber septa and a syringe, were used for the reaction. The figure Sa explains the schematic illustration of the testing process. Ten milligrams of catalyst were weighed and transferred into the quartz vial, filled with 5 ml of 0.5 M $KHCO_3$ solution. The catalyst was dispersed into the solution using small magnetic beads. The vials were closed with rubber septa and a syringe needle was used to feed gas enter the vials in a controlled fashion. The vials were put inside the Parr vessel and the remaining

empty space inside was filled with glass wool to support the vials. The vessel was flushed 3 times using the feed gas mixture to flush out the oxygen gas from vessel. The vessel was pressurized till 40 bar and put inside the preheated oil bath at 40 °C. An external temperature indicator was attached to the Vessel's thermocouple to monitor the inside temperature throughout the course of experiment. Upon completion of experiment the product solution was removed from vials and centrifuged at a rate of 1500 rpm for 5 mins to remove catalyst. The products solution was analysed by Agilent HPLC, with RID and VWD as the detector.

Product Analysis

The liquid products were analysed by HPLC (Agilent 1220 Infinity II LC system). The HPLC compartment contains autosampler, quaternary pump, column, refractive index detector (RID), and variable wavelength detector (VWD). Hi-Plex H column has been used to detect the organic liquid products like acids and alcohols. The flow rate through the Hi-Plex H column is kept at 0.5 ml/min while analysing samples. Five mM H_2SO_4 is used as the mobile phase during analysis. The column temperature was kept at 50 °C. VWD uses a light signal to detect chromophores in the analytes. It can be used the products include ketones/carboxylic acids/aldehydes. Acquisition frequency is given as 10 Hz with a peak width of 0.05 min. It is good enough to record sufficient data points. RID is the primary detector in this HPLC configuration. It is a highly sensitive detector which works based on the difference in refractive index of the sample and analyte.

Computational Details

All DFT calculations were performed within Perdew-Becke Ernzerhof (PBE)[6] exchange-correlation functional implemented in the Viana Ab Initio Simulation Package (VASP).[7, 8] Plane augmented pseudopotential[9] that represents the interaction between ionic cores and valence electrons were used with a kinetic energy cutoff of 400 eV to truncate the plane-wave basis. A convergence threshold of 0.03 eV/Å is accounted for forces on the atoms for ionic minimization. The correction to long-range dispersion interactions was included by employing the D3 correction method by Grimme et al.[10] The Monkhorst-Pack mesh[11] k-points of (3 × 3 × 1) is used for the p(3 × 3) surface slab of monometallic Pd, Ni and bimetallic PdNi and PdAg containing four atomic layers, with a vacuum thickness of 14 Å. The atoms in the top two layers were allowed to relax while the bottom two layers were fixed at the bulk equilibrium position.

The Adsorption energy (E_{ads}) was calculated as:

$$E_{ads} = E_{slab+x} - (E_{slab} + E_x)$$

Where E_{slab+x}, E_{slab} and E_x are the total energy of slab with adsorbate, the energy of bare slab, and the energy of adsorbate in the gas phase respectively. The transition state calculations were done using the Nudge Elastic Band (NEB) method implemented in VASP.

Tables

Table S1. ICP-OES data of different Pd-Ni, Pd-Ag and Pd-Co system on different Schiff base functionalized SBA-15.

Catalyst	Wt % of Metals	
	Pd	Ni or Co or Ag
Pd-Ni/APTES-GLU-D (200 μmol)	9.40	8.67
Pd-Co/APTES-GLU-D (200 μmol)	9.36	9.74
Pd-Ag/APTES-GLU-D (200 μmol)	9.83	9.4
Pd-Ag/APTES-BUT-D (200 μmol)	9.11	9.5
Pd-Ag/APTES-GLU-Ex. (200 μmol)	9.62	9.3
Pd-Ni/APTES-GLU-Ex. (200 μmol)	9.58	9.16
Pd-Ag/APTES-BUT-Ex. (200 μmol)	9.36	8.94
Pd-Ni/APTES-BUT-Ex. (200 μmol)	9.2	9.10
Pd_3Ni/APTES-GLU-D (200 μmol)	14.81	4.93
$PdNi_3$/APTES-GLU-Ex. (200 μmol)	4.87	14.94
Pd_3Ag/APTES-GLU-D (200 μmol)	14.95	4.63
$PdAg_3$/APTES-GLU-D (200 μmol)	4.83	14.88
PdAg/APTES-GLU-D (20 μmol)	0.92	0.93
PdNi/APTES-GLU-D (20 μmol)	0.89	0.94

Table S2. Textural properties of silica and impregnated catalyst.

Sample	Surface Area/m^2g^{-1}	Pore Volume/cm^3g^{-1}	Avg. Pore Diameter/nm
SBA-15	665	0.95	7.2
SBA-15/APTES-GLU-D	124	0.16	45
SBA-15/APTES-GLU-Ex.	116	0.14	58
SBA-15/APTES-BUT-D	124	0.18	39

Table S3. CO_2 uptake results obtained from Dynamic uptake experiment

Adsorbent Materials	CO_2 Uptake (ml $CO_2/g_{sorbent}$)		Total Uptake	
	Breakthrough	Post-Breakthrough	(ml $CO_2/g_{sorbent}$)	(mg $CO_2/g_{sorbent}$)
APTES-BUT-D/SBA-15	0.69	0.17	0.86	1.69
APTES-GLU-D/SBA-15	1.17	0.59	2.29	4.5

APTES-BUT-Ex/SBA-15	0.39	1.49	1.88	3.69
APTES-GLU-Ex/SBA-15	0.29	0.19	0.48	0.94

Table S4. CO_2 uptake comparison in static mode of experiment in different temperatures

Adsorbent Materials	**CO_2 Uptake (ml $CO_2/g_{sorbent}$)**		
	40 °C (303 K)	**25 °C (298 K)**	**0 °C (273 K)**
APTES-BUT-D/SBA-15	1.43	1.4	2.68
APTES-GLU-D/SBA-15	3.4	5.05	5.72
APTES-BUT-Ex/SBA-15	2.64	2.58	1.88
APTES-GLU-Ex/SBA-15	1.4	1.67	2.88

Table S5. Isosteric heats of SBA-15 functionalized APTES-GLU materials

Support Material	**Q_{st} (kJ/mol)**
APTES-GLU-D	48.02
APTES-GLU-Ex	22.945
APTES-BUT-D	55.509
APTES-BUT-Ex	45.478

Table S6: CO_2 reduction test results of monometallic (Pd, Ni, Co, and Ag) (200 µM) on APTES-GLU-D/SBA-15 support at 40 ºC and 40 Bar.

Catalyst	**Reaction Condition**			**TON (mol_{FA}/mol_{Pd})**	**TOF (h^{-1})**
	Temperature (°C)	**Pressure / CO_2:H_2 (Bar)**	**Time (h)**		
Pd/APTES-GLU-D	40	20/20	12	51.6	4.3
Ag/APTES-GLU-D	40	20/20	12	0.15	0.012
Ni/APTES-GLU-D	40	20/20	12	0.19	0.016
Co/APTES-GLU-D	40	20/20	12	0.11	0.009

Table S7: CO_2 reduction test results of Bi-metallic (Pd-Co, Pd-Ni, and Pd-Ag) (200 µM) on APTES-GLU-D/SBA-15 support at 40 ºC and 40 Bar.

Catalyst	**Reaction Condition**			**TON (mol_{FA}/mol_{Pd})**	**TOF (h^{-1})**
	Temperature (°C)	**Pressure / CO_2:H_2 (Bar)**	**Time (h)**		
Pd-Ni/APTES-GLU-D	40	20/20	12	63.2	5.3
Pd-Co/APTES-GLU-D	40	20/20	12	11.1	0.92

Pd-Ag/APTES-GLU-D	40	20/20	12	146	12.2

Table S8: CO_2 reduction test results of Pd-Ni/APTES-GLU-D (200 μM) at different temperature and 40 Bar.

Catalyst	**Reaction Condition**			**TON** (mol_{FA}/mol_{Pd})	**TOF** (h^{-1})
	Temperature (℃)	**Pressure / CO_2:H_2 (Bar)**	**Time (h)**		
Pd-Ni/APTES-GLU-D	30	20/20	12	47.5	3.95
Pd-Ni/APTES-GLU-D	40	20/20	12	63.2	5.3
Pd-Ni/APTES-GLU-D	50	20/20	12	60.6	5

Table S9: CO_2 reduction test results of Pd-Ni/APTES-GLU-D (200 μM) at different pressure and 40 ºC.

Catalyst	**Reaction Condition**			**TON** (mol_{FA}/mol_{Pd})	**TOF** (h^{-1})
	Temperature (℃)	**Pressure / CO_2:H_2 (Bar)**	**Time (h)**		
Pd-Ni/APTES-GLU-D	40	15/15	12	56.5	4.7
Pd-Ni/APTES-GLU-D	40	20/20	12	63.2	5.3

Table S10: CO_2 reduction test results of Pd-Ni (200 μM) on different supports at 40 ºC and 40 Bar.

Catalyst	**Reaction Condition**			**TON** (mol_{FA}/mol_{Pd})	**TOF** (h^{-1})
	Temperature (℃)	**Pressure / CO_2:H_2 (Bar)**	**Time (h)**		
Pd-Ni/APTES-GLU-D	40	20/20	12	63.2	5.3
Pd-Ni/APTES-GLU-Ex.	40	20/20	12	9.9	0.83
Pd-Ni/APTES-BUT-D	40	20/20	12	20.2	1.7
Pd-Ni/APTES-BUT-Ex.	40	20/20	12	28.6	2.4

Table S11: CO_2 reduction test results of Pd_xNi_{1-x} (Pd_3Ni, PdNi, and $PdNi_3$) and Pd_xAg_{1-x} (Pd_3Ag, PdAg and $PdAg_3$) (200 μM) on APTES-GLU-D/SBA-15 support at 40 ºC and 40 Bar.

Catalyst	**Reaction Condition**			**TON** (mol_{FA}/mol_{Pd})	**TOF** (h^{-1})
	Temperature (℃)	**Pressure / CO_2:H_2 (Bar)**	**Time (h)**		
Pd_3Ni/APTES-GLU-D	40	20/20	12	4.75	0.39
PdNi/APTES-GLU-D	40	20/20	12	63.2	5.3
$PdNi_3$/APTES-GLU-D	40	20/20	12	2.3	0.2
Pd_3Ag/APTES-GLU-D	40	20/20	12	7.4	0.61
PdAg/APTES-GLU-D	40	20/20	12	146	12.2

$PdAg_3$/APTES-GLU-D	40	20/20	12	4.5	0.38

Table S12: CO_2 reduction test results of Pd-Ni/APTES-GLU-D with different concentration at 40 ºC and 40 Bar

Catalyst	**Reaction Condition**			**TON** (mol_{FA}/mol_{Pd})	**TOF** (h^{-1})
	Temperature (℃)	**Pressure / CO_2:H_2 (Bar)**	**Time (h)**		
Pd-Ni/APTES-GLU-D (20)	40	20/20	12	132.2	11.01
Pd-Ni/APTES-GLU-D (200)	40	20/20	12	63.2	5.3
Pd-Ni/APTES-GLU-D (2000)	40	20/20	12	5.53	0.46

Table S13: CO_2 reduction test results on Pd-Ni/APTES-GLU-D (20 μM) with different time interval at 40 ºC and 40 Bar.

Catalyst	**Reaction Condition**			**TON** (mol_{FA}/mol_{Pd})	**TOF** (h^{-1})
	Temperature (℃)	**Pressure / CO_2:H_2 (Bar)**	**Time (h)**		
Pd-Ni/APTES-GLU-D	40	20/20	12	132.2	3.95
Pd-Ni/APTES-GLU-D	40	20/20	0.25	53	212
Pd-Ag/APTES-GLU-D	40	20/20	12	181.5	15.1
Pd-Ag/APTES-GLU-D	40	20/20	0.25	11	44.6

Figures

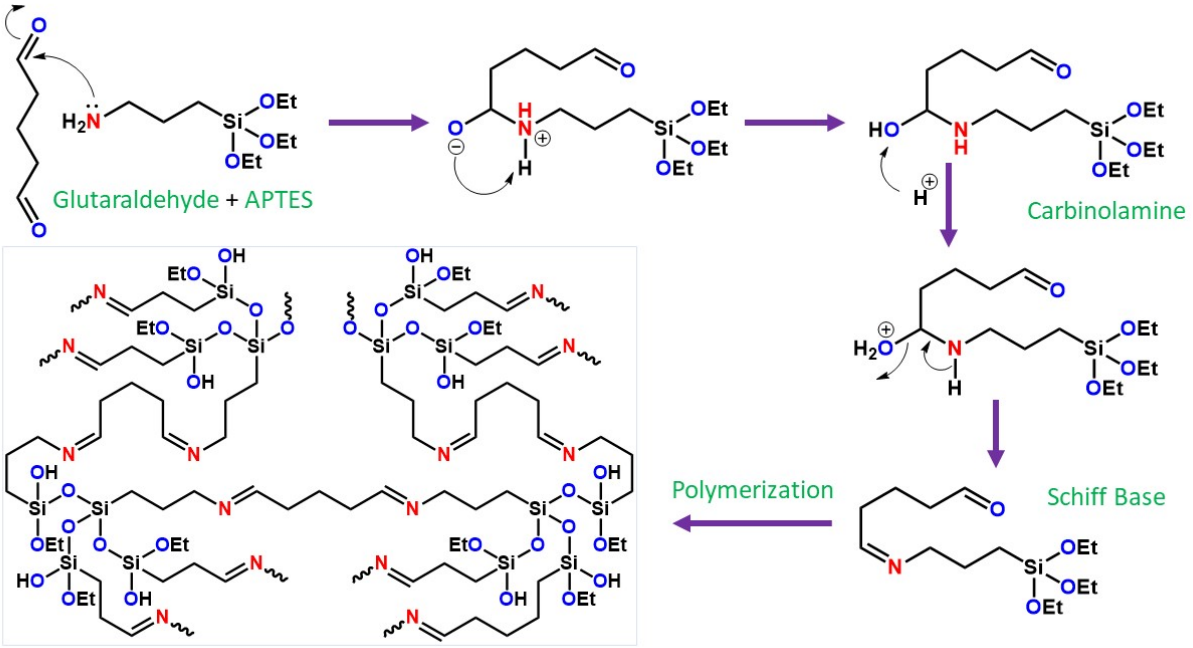

Figure S1. Schematic representation of condensation of glutaraldehyde with APTES.

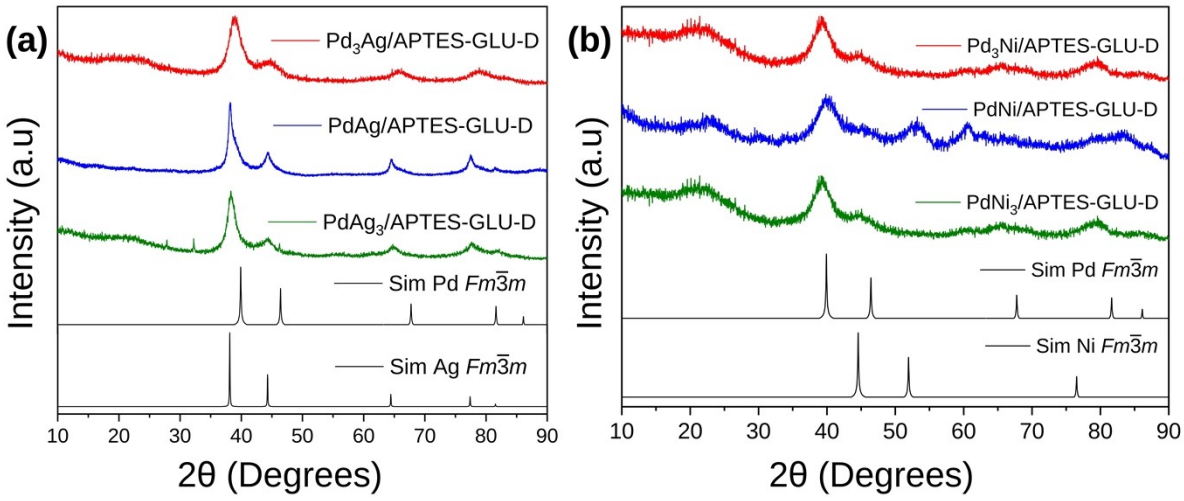

Figure S2. (a) XRD patterns of Pd-Ag/SBA-15/APTES-GLU-D and (b) Pd-Ni/SBA-15/APTES-GLU-D compared with corresponding metal nanoparticles.

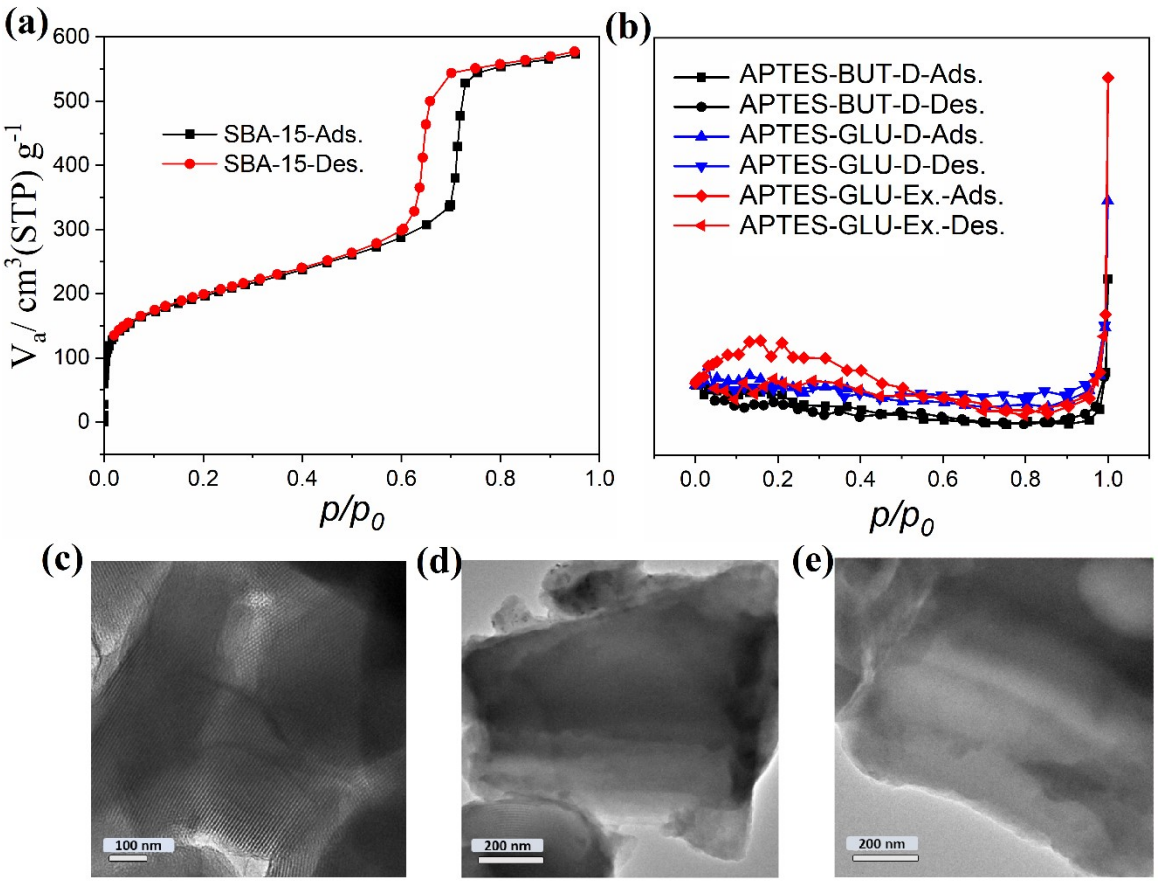

Figure S3. N_2 adsorption-desorption spectra of (a) SBA-15, (b) APTES-GLU-D, APTES-BUT-D and APTES-GLU-Ex combined. (c) TEM image of SBA-15, (d) TEM image of APTES-GLU-D and (e) APTES-GLU-Ex.

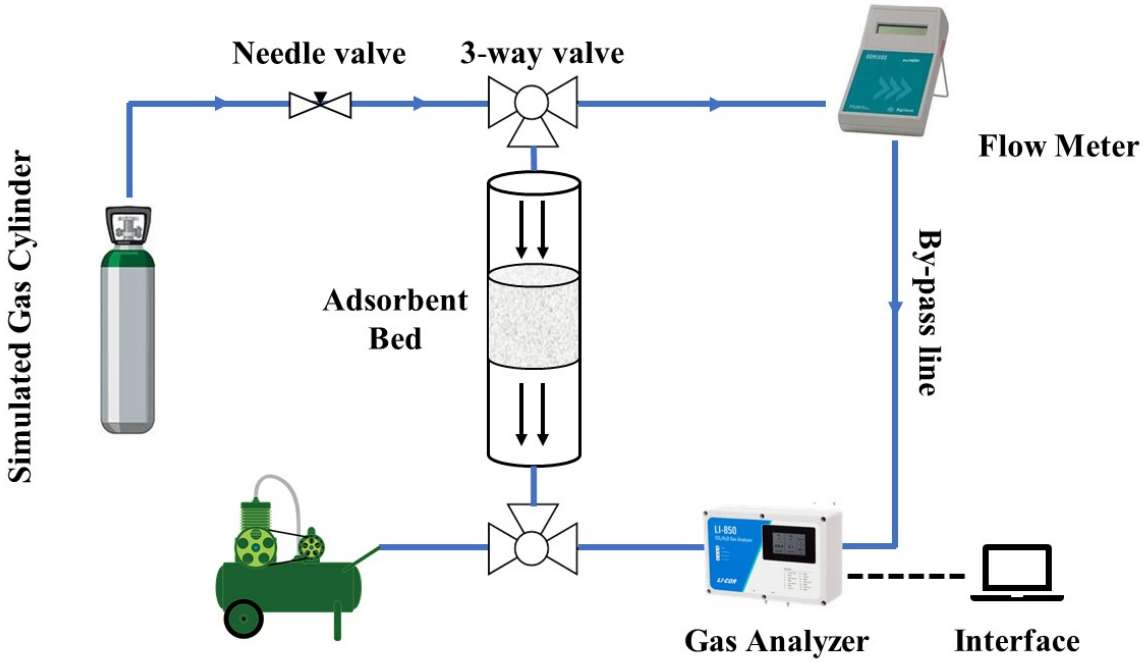

Figure S4. Schematic representation of dynamic uptake experiment setup.

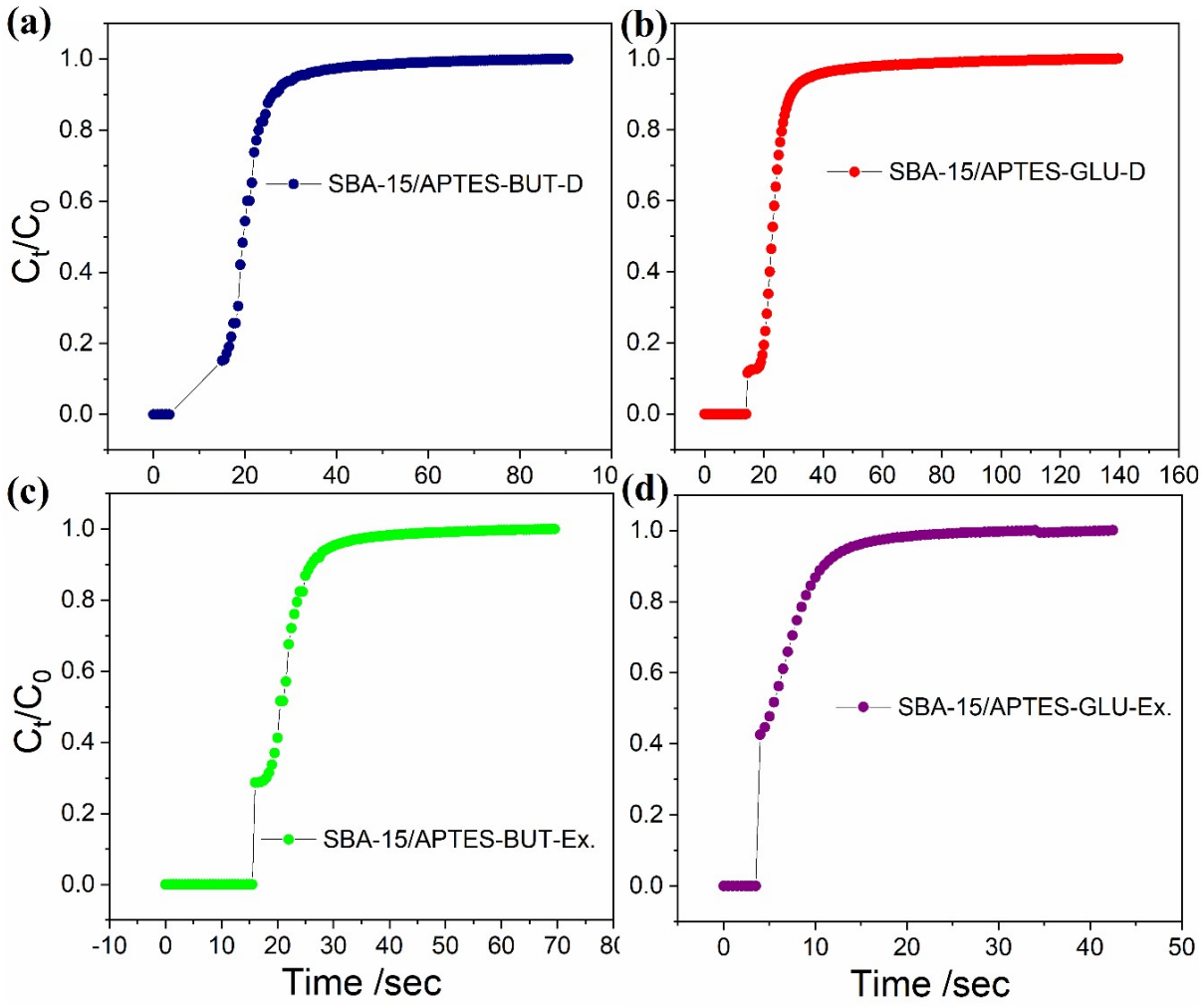

Figure S5. CO_2 uptake profile obtained from dynamic uptake experiment; (a) Direct Butyraldehyde APTES/SBA-15, (b) Direct Glutaraldehyde APTES/SBA-15, (c) Indirect Butyraldehyde APTES/SBA-15, (d) Indirect Glutaraldehyde APTES/SBA-15.

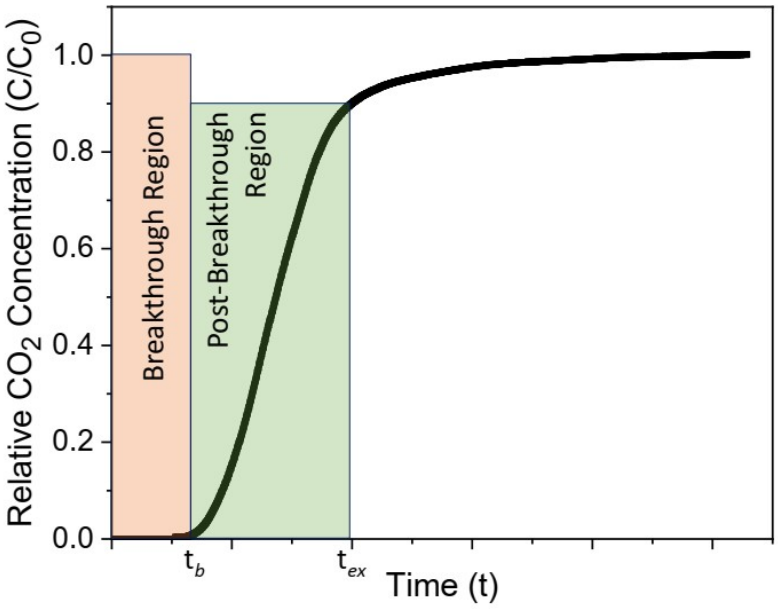

Figure S6. CO_2 Uptake Profile: Relative Conc. vs Time

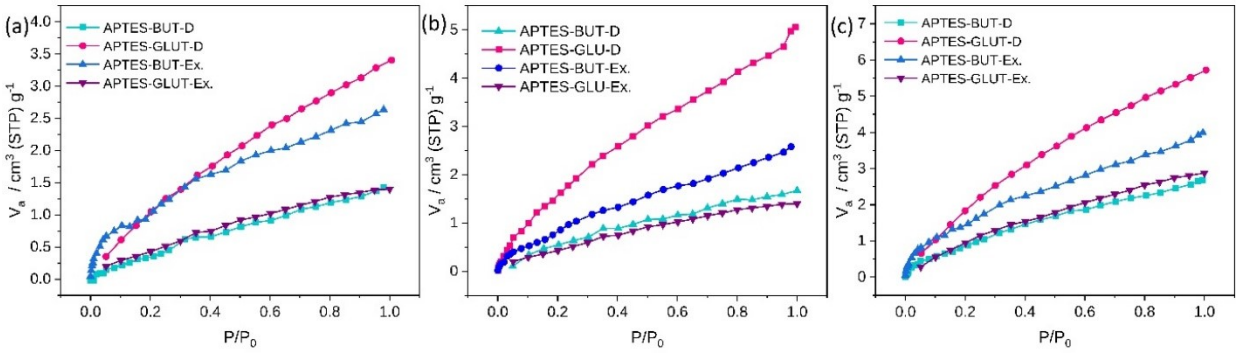

Figure S7. CO_2 uptake profile obtained from static uptake experiment at (a) 40 ºC, (b) 25 ºC & 0 ºC.

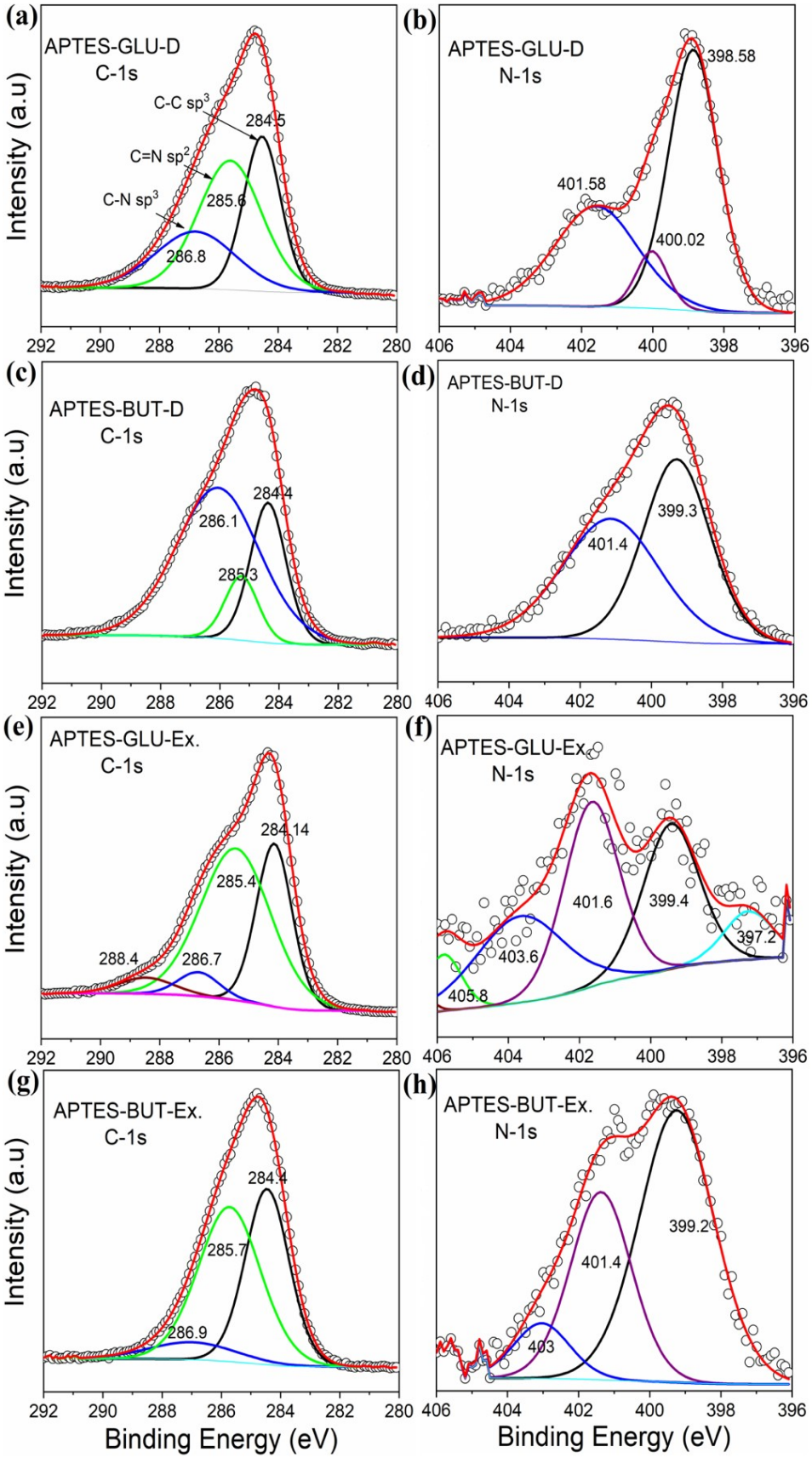

Figure S8. XPS spectra of (a) C-1s and (b) N-1s spectra of APTES-GLU-D, XPS spectra of (c) C-1s and (d) N-1s spectra of APTES-BUT-D, (e) C-1s and (f) N-1s spectra of APTES-GLU-Ex, (g) C-1s and (h) N-1s spectra of APTES-BUT-Ex.

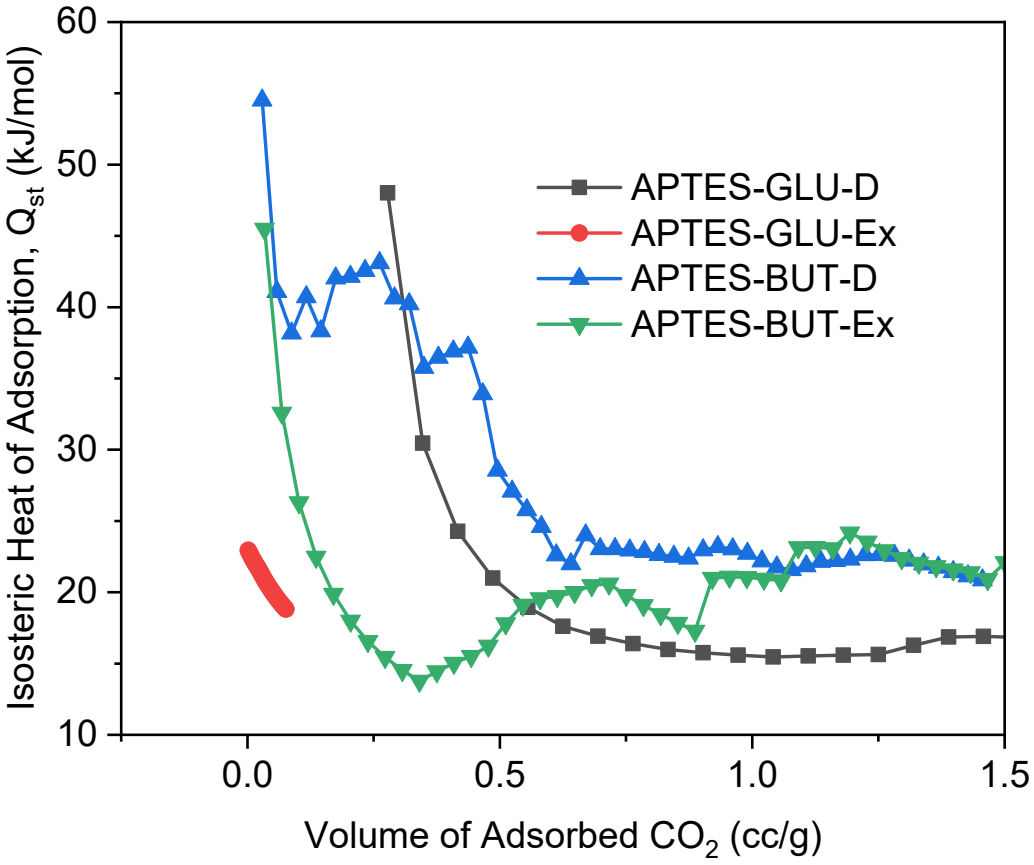

Figure S9. Comparison of isosteric heat of adsorption of APTES-GLU-D, APTES-GLU-Ex, APTES-BUT-D and APTES-BUT-Ex.

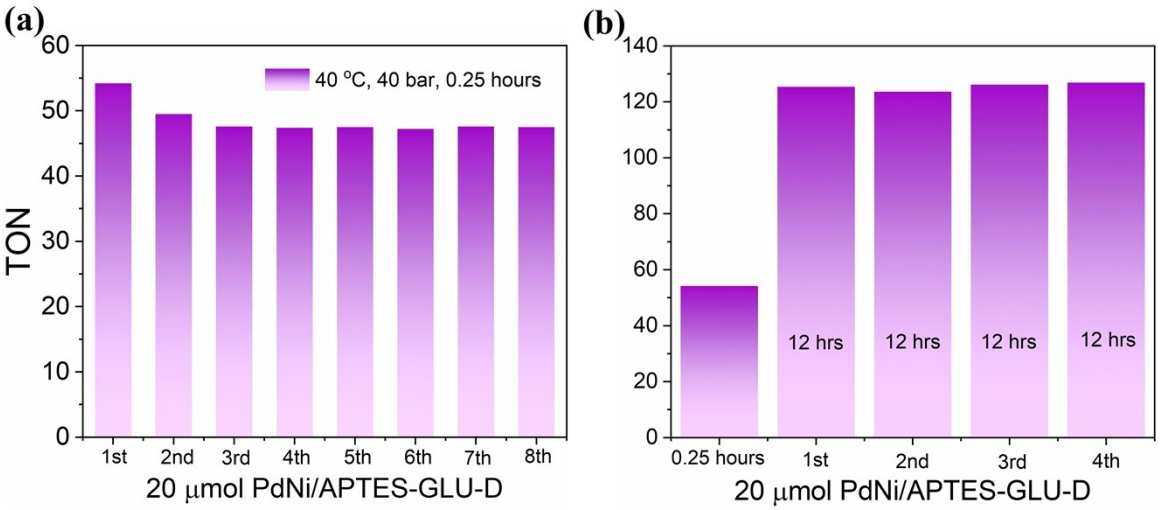

Figure S10. Catalyst recycle test at an interval of (a) 0.25 hours & (b) 12 hours.

Reference

1. E. M. Björk, *J. Chem. Educ.*, 2017, **94**, 91-94.
2. D. Zhao, Q. Huo, J. Feng, B. F. Chmelka and G. D. Stucky, *J. Am. Chem. Soc.*, 1998, **120**, 6024-6036.
3. S. Masuda, K. Mori, Y. Kuwahara, C. Louis and H. Yamashita, *ACS Appl. Energy Mater.*, 2020, **3**, 5847-5855.
4. B. Ravel and M. Newville, *J. Synchrotron Radiat.*, 2005, **12**, 537-541.
5. Z. Chowdhury, S. Zain, A. Rashid, R. Rafique and K. Khalid, *J. Chem.*, 2013, **2013**.
6. J. P. Perdew, K. Burke and M. Ernzerhof, *Phys. Rev. Lett.*, 1996, **77**, 3865-3868.
7. G. Kresse and J. Furthmüller, *Phys. Rev. B*, 1996, **54**, 11169-11186.
8. G. Kresse and J. Furthmüller, *Comput. Mater. Sci.*, 1996, **6**, 15-50.
9. P. E. Blöchl, *Phy. Rev. B*, 1994, **50**, 17953-17979.
10. S. Grimme, J. Antony, S. Ehrlich and H. Krieg, *J. Chem. Phys.*, 2010, **132**, 154104.
11. H. J. Monkhorst and J. D. Pack, *Phy. Rev. B*, 1976, **13**, 5188-5192.